Point defects in beryllium-doped GaN

Mykhailo Vorobiov, Oleksandr Andrieiev, Denis O. Demchenko, and Michael A. Reshchikov

Phys. Rev. B **104**, 245203 — Published 8 December 2021

DOI: 10.1103/PhysRevB.104.245203

Point Defects in Beryllium Doped GaN

Mykhailo Vorobiov,* Oleksandr Andrieiev, Denis O. Demchenko, and Michael A. Reshchikov

Department of Physics, Virginia Commonwealth University,

Richmond, Virginia 23284-2000, USA

Abstract

Detailed analysis of the defect-related photoluminescence (PL) in semi-insulating and n-type Be-doped GaN samples grown by molecular beam epitaxy is presented. The dominant PL bands in these samples are the ultraviolet (UVL_{Be}), yellow (YL_{Be}), red (RL_{Be}), and green (GL2) bands. The UVL_{Be} band is caused by electron transitions via the $0/-$ level of the Be_{Ga} acceptor located at 113 meV above the valence band. The UVL_{Be} band is quenched above 60 K, and the quenching is tunable by excitation intensity. The quenching of the YL_{Be} above 200 K is likely related to an acceptor level at 0.3 eV. In semi-insulating samples, the quenching temperature is tunable with the intensity of the excitation laser. Based on the first-principles calculations, the YL_{Be} band is preliminarily attributed to the Be_{Ga}-V_N-Be_{Ga} complex. The new RL_{Be} band is attributed to the internal transition in the Be_{Ga}-V_N complex with a deep $+/0$ transition level at about 0.95 eV.

I. INTRODUCTION

Gallium nitride (GaN) is one of the most important semiconductors for modern opto-electronics, particularly blue and ultraviolet light-emitting devices. The technology of these devices relies heavily on the doping processes to create regions with opposite conductivity types. While n-type GaN can be obtained relatively easily [1], achieving reliable p-type conductivity proved to be challenging. Indeed, the only known p-type dopant for GaN is Mg incorporated into the Ga site (Mg_{Ga}). The defect forms a $0/-$ transition level at 223 meV above the valence band maximum (VBM) [2]. Such ionization energy is too high to produce significant concentrations of holes (above mid-10^{18} cm^{-3}) [3]. An increase in hole concentration to the production-acceptable levels is commonly achieved by heavy doping ([Mg] $\sim 10^{20}$ cm^{-3}). High concentrations of Mg create significant lattice distortions leading to potential fluctuations and may contribute to scattering that lowers mobility. In addition, Mg acceptors are often heavily compensated by donors such as nitrogen vacancy (V_N). As a result, p-type GaN:Mg samples are often poorly conductive.

A few experimental works indicate that Beryllium (Be) could be a promising alternative for p-type doping of GaN [4, 5]. Interestingly, the hole concentration of 8×10^{19} cm^{-3} has been reported [6] in Be-implanted Mg-doped GaN. However, no reliable and reproducible

* vorobiovm@vcu.edu

p-type conductivity in Be-doped GaN has been demonstrated to date. Calculations show that Be, can be incorporated into interstitial sites (Be_i) even under N-rich conditions [7]. This leads to self-compensation by Be_i double donors, which limits p-type conductivity [8].

The first-principles calculations initially predicted Be_{Ga} to be an acceptor with an ionization energy of 0.2 eV above the VBM [9–12]. More recent calculations [13, 14] resulted in a $0/-$ transition level at 0.55-0.65 eV above the VBM. Such a deep level is an example of a small polaron [15]: the hole is self-trapped due to significant lattice distortions around the Be_{Ga} center. The localization occurs at the nearest neighbor nitrogen atom that is moved ~ 0.7 Å from its equilibrium position [16]. Recently, using photoluminescence (PL) measurements and hybrid functional calculations, we showed that Be_{Ga} in GaN also forms a shallow acceptor level at 113 ± 5 meV above the VBM [7]. Electron-hole recombination through this shallow level produces an ultraviolet luminescence band (UVL_{Be}, hereafter) in the PL spectra. The band has a zero-phonon line (ZPL) at 3.38 eV and a series of LO phonon replicas with the Huang-Rhys factor of about 0.2. At low temperatures, the transitions proceed via the shallow donor-acceptor pair (DAP) mechanism. With increasing temperature from 18 to 50 K, the transitions transform from the DAP-type into transitions from the conduction band minimum (CBM) to the same acceptor (eA transitions). Our calculations [7] also predict a small polaron state existing along with the shallow state. However, the former is not observed in the PL experiments because of the significantly lower hole-capture coefficient than that for the shallow state [7].

Another PL band commonly observed in GaN:Be layers grown by molecular beam epitaxy (MBE), namely the YL_{Be} band, is reported to have a maximum at 2.1-2.2 eV [3, 17]. A similar strong yellow luminescence band appears in bulk crystals containing high concentrations of Be and oxygen ($\sim 10^{19}$ cm^{-3}), and was attributed to the Be_{Ga}-O_N complex [18]. Lamprecht et al. [19] suggested that the yellow band in these samples consists of three unresolved bands, and one of them (with a maximum at 2.08 eV) decays extremely slowly with time after the laser is switched off (with the lifetime exceeding 1 second at room temperature).

A red luminescence band from GaN:Be has been observed in Ref. [20], but no detailed characterization has been reported. The band appeared after annealing the samples at 900 °C in pure N_2 ambient for 2 hours. As will be shown below, in samples where the red luminescence is not obscured by the yellow emission, it is accompanied by the green

band known as GL2. The GL2 band is attributed to the internal transition in the V_N [21]. The GL2 band maximum is located at 2.35 eV, with the ZPL expected at 2.85 eV and the Huang-Rhys factor of 26.5.

In this work, we analyze in detail the PL data from Be-doped GaN grown by MBE and identify PL bands observed in these samples by comparing the properties of the PL bands with predictions of the first-principles calculations.

II. METHODS

The Be-doped GaN layers were grown by MBE on c-plane sapphire substrates at the West Virginia University [22], see Table I. About ten Ga-polar samples with the thickness of the GaN:Be layer of about 1 μm were grown on top of the ~ 0.1 μm-thick undoped GaN. Three N-polar samples (0020-i with i = 1, 2, 3) were deposited directly on sapphire. Some of the samples were annealed at 900°C in nitrogen ambient (marked with index b in Table I). Positron annihilation measurements, conducted on these samples, showed that the Be predominantly incorporated into Ga sites, forming the Be_{Ga} defects with the concentration of at least 10^{17} cm^{-3}, possibly as a part of a complex involving oxygen or hydrogen [8]. Secondary ion mass-spectrometry (SIMS) confirmed the presence of Be with concentrations ranging from 10^{17} to 10^{20} cm^{-3} in different samples (Table I). Further details on the growth of the samples can be found in [23]. Only one sample (N-polar sample 0020-1) was conductive n-type, which was established from analysis of the PL data and Hall effect measurements, other samples were semi-insulating. Some samples (see Table I) were grown under atomic H and In surfactants under electron beam irradiation aimed to enhance the incorporation of Be into Ga sites [23].

The steady-state PL (SSPL) was excited with a He-Cd laser (25 mW, 325 nm), dispersed by the 1200 rules/mm diffraction grating in a 0.3 m monochromator, and detected by a Peltier-cooled photomultiplier tube. The neutral density filters were used to attenuate the excitation intensity in the range from 10^{-5} to 0.13 W/cm^2. Excitation intensities up to 100 W/cm^2 were achieved by focusing the laser beam. The PL measurements were corrected for the optical elements and detector sensitivities with a calibrated tungsten-halogen lamp. The spectra measured as a function of wavelength, λ, were multiplied by λ^3 in order to plot the spectra in units proportional to the number of emitted photons as a function of photon

TABLE I. Parameters of Be-doped GaN samples. Samples with index "b" were annealed at 900°C. Samples 0406b and 0410b contained two regions with drastically different properties.

Sample	Doping		PL QE (%)				$N_A - N_D$ (cm^{-3}) from quenching of PL	
	[Be] (cm^{-3})	Other	UVL_{Be}	YL_{Be}	RL_{Be}	GL2	UVL_{Be} [a)]	YL_{Be} [b)]
0406a	1×10^{19}		< 0.00003	0.8	0.6			
0406b1	1×10^{19}		< 0.0001	0.7	0.01			
0406b2	1×10^{19}		< 0.0001		0.5	0.02		
0408a	5×10^{17}		0.0001	20	0.0002			1×10^{17}
0408b	5×10^{17}		0.06	20	0.007			1×10^{16}
0410a	1×10^{18}		< 0.0003	7	0.002			
0410b1	1×10^{18}		0.03	5				
0410b2	1×10^{18}		0.03	-	3	0.2		
0411a	4×10^{18}		< 0.00001	5	< 0.0001			1×10^{17}
0411b	4×10^{18}		< 0.0001	-	10	2		
0413a	1×10^{18}	H	< 0.00003	0.5	0.07			
0413b	1×10^{18}	H	< 0.0001	-	10	3		
0414a	1×10^{19}	H	0.005	2	0.007			4×10^{17}
0414b	1×10^{19}	H	0.5	50	0.03		6×10^{15}	1×10^{17}
0415b	1×10^{20}	H	0.04	1.5	1			
0416b	1×10^{18}	In	0.12	-	10	2	4×10^{17}	
0417a	1×10^{19}	In	< 0.00003	-	10	1		
0417b	1×10^{19}	In	< 0.00003	1.4	0.01			
0418a	1×10^{20}	In	0.005	5	0.002			1×10^{17}
0418b	1×10^{20}	In	0.01	-	1	0.2		
0419a	2×10^{18}		< 0.0001	10	< 0.0001			3×10^{17}
0419b	2×10^{18}		0.05	-	10	1		
0020-1	7×10^{18}		< 0.001	25	< 0.01			
0020-2	7×10^{18}		0.2	30	0.05		2×10^{15}	
0020-3	7×10^{18}		0.1	15	0.01			

[a)] From Eq. (3) with $C_{pA} = 10^{-6}$ cm^3/s

[b)] From Eq. (3) with $C_{pA} = 4 \times 10^{-7}$ cm^3/s

energy [24]. The time-resolved PL (TRPL) was excited with a pulsed nitrogen laser (pulse duration 1 ns, 6 Hz repetition rate, and photon energy 3.68 eV). The signal was analyzed with an oscilloscope. A closed-cycle optical cryostat was used to carry out measurements in the temperature range from 18 to 320 K. The samples were studied under identical conditions. The PL quantum efficiencies (QE) for each PL band were found by comparison of the integrated intensity with that from calibrated GaN samples. The calibrated samples were grown by the metal-organic vapor phase epitaxy method and doped with C and Si. The Carbon-related YL1 band in these samples has a very high internal quantum efficiency (IQE) η_{YL1} that is determined with high accuracy. The relative QE of an unknown band η_u can be determined as $\eta_u = (I_u/I_{\mathrm{YL1}})\eta_{YL1}$, where I_u and I_{YL1} are the integrated intensities of the unknown and the calibration YL1 bands, respectively. Other details can be found in Refs. [24, 25].

Theoretical calculations were performed using the Heyd-Scuseria-Ernzerhof (HSE) hybrid functional [26]. The HSE functional was tuned to fulfill the generalized Koopmans condition for the $\mathrm{Mg_{Ga}}$ acceptor in GaN (fraction of exact exchange is 0.25, the range separation parameter is 0.161 $\mathrm{Å^{-1}}$) [27]. Our tests show that the generalized Koopmans condition is fulfilled by this parametrization of HSE for the $\mathrm{Be_{Ga}}$ acceptor as well. In calculations of the optical transition levels, an experimental bandgap of GaN (3.5 eV) is used. Since the above parametrization of HSE slightly underestimates the bandgap (3.22 eV), to compare the defect optics with the experiment we essentially perform a scissor operation and move the conduction band up to the correct value. Calculations were performed in 300-atom hexagonal supercells at the $\mathbf{\Gamma}$-point, with plane-wave energy cutoffs of 500 eV. All defect atomic structures were relaxed within HSE to minimize forces to 0.05 eV/Å or less. Spurious electrostatic interactions in calculated total energies were corrected using the Freysoldt-Neugebauer-Van de Walle approach [28, 29]. Defect formation energies were calculated following the procedure outlined in Ref. [30]. Adiabatic potentials used to plot the configuration coordinate diagrams were obtained by fitting into HSE computed total energies using harmonic approximation and mapping the atomic displacements ΔR_i onto the configuration coordinate Q as $\Delta Q^2 = \sum_{i,x,y,z} m_i \Delta R_i^2$, where m_i are the atom masses. Elemental chemical potentials used in defect formation energy calculations were obtained from the total energies of the GaN growth competing phases. For example, in a nitrogen-rich growth regime the chemical potential of nitrogen is set to $\mu_N(\mathrm{N_2})$ while that of gallium is

set to μ_{Ga}(Ga metal) + ΔH_f(GaN), where ΔH_f(GaN) is the formation enthalpy of GaN (computed to be −1.2 eV). The chemical potential of oxygen is assumed to be limited by the formation of gallium oxide Ga_2O_3. In turn, in the presence of oxygen, the formation of beryllium defects is assumed to be limited by the growth of beryllium oxide BeO. Binding energies of defect complexes are calculated as the formation energy differences between the complex and its constituents in the lowest energy charge states.

III. RESULTS AND DISCUSSION

A. Main photoluminescence bands in Be-doped GaN

We observed four major defect-related bands in PL spectra from Be-doped GaN samples. Representative low-temperature PL spectra from two samples are shown in Fig. 1. The main defect-related PL bands are the UVL_{Be} band with the strongest peak at 3.38 eV, the broad YL_{Be} band with a maximum at about 2.2 eV, the RL_{Be} band with a maximum at about 1.8 eV, and the GL2 band with a maximum at 2.33 eV and full width at half maximum of 0.25 eV. The positions and shapes are well reproduced in different samples. The estimated QEs of these bands are given in Table I. The GL2 band is attributed to the V_N defect [21], while three other PL bands are related to Be as will be shown below. In some samples, additional features could be observed in PL spectra at certain temperatures or excitation intensities, such as the Mg-related UVL_{Mg} band with the strongest peak at 3.28 eV and a broad blue band, which overlapped with the YL_{Be} band. These features and the near-band-edge (NBE) emission are beyond the scope of this paper.

In two samples (0406b and 0410b), the optical properties varied greatly across the sample surface within the 5-mm sample size. Similar to what we observed earlier in Mg-doped MBE GaN [21], two regions with different PL spectra were observed, and the boundary between these regions was very sharp. An example is shown in Fig. 2 for sample 0410b.

We were unable to find a clear correlation between the appearance of defect-related PL bands and the following properties of the samples: concentration of Be, co-doping with H or In, and the sample polarity (see Table I). In particular, the bright YL_{Be} band was observed in 14 Ga-polar samples (including annealed samples) and all three N-polar samples. It was also very strong in the only conductive n-type sample (0020-1). The UVL_{Be} band

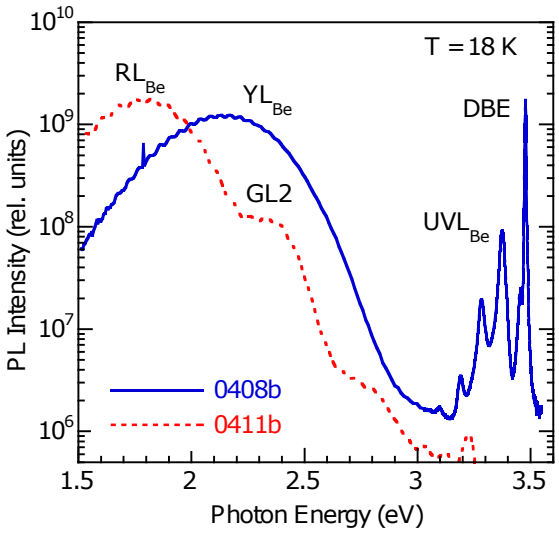

FIG. 1. (Color online) The representative PL spectra from samples 0408b and 0411b dominated by the red (RL_{Be}) and yellow (YL_{Be}) bands, respectively. The ultraviolet PL band (UVL_{Be}) and the exciton band with a sharp DBE peak are relatively strong in sample 0408b. Measurements were carried out in identical conditions at $T = 18$ K and under excitation intensity $P_{exc} = 0.13$ W/cm^2. The small-amplitude oscillations are due to the Fabry-Perot interference inside the GaN layer. The feature at about 1.7 eV is the PL emission from the sapphire substrate.

was observed in 9 out of 17 samples with the strong YL_{Be} band and in 4 out of 8 samples with the strong GL2 band. Nevertheless, some regularities were noticed: (i) with almost no exceptions, the UVL_{Be} band appeared in GaN:Be samples after they were annealed at 900 ^{o}C in nitrogen ambient (the samples containing letter b in the name). (ii) In all 8 samples with the GL2 band, the RL_{Be} band was very strong and the YL_{Be} band was absent (Table I). This rule is emphasized in samples 0406b and 0410b, where the YL_{Be} band suddenly disappears in the region where the GL2 and RL_{Be} bands are strong (Fig. 2). Note that in samples with the dominant YL_{Be} band, a weak red band could be detected at $T > 200$ K after the quenching of the YL_{Be} band. In Table I, the QE of this red band is given in the column labeled RL_{Be}. However, because of its low intensity, we could not confirm or reject the assumption that this red band is RL_{Be}.

It is important to note that no correlation could be found between the RL_{Be} and UVL_{Be} bands or between the YL_{Be} and UVL_{Be} bands. The ratio of peak intensities, YL_{Be}/UVL_{Be} or RL_{Be}/UVL_{Be} varied from 10^{-3} to 10^3 across different samples. This suggests that these

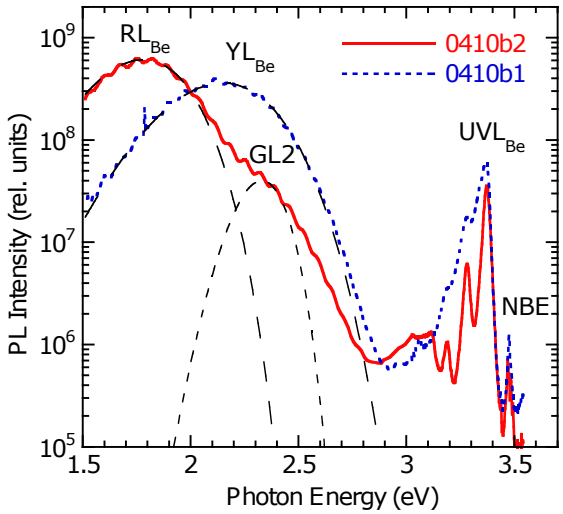

FIG. 2. (Color online) PL spectra at $T = 18$ K and $P_{exc} = 0.13$ W/cm^2 from two regions of the sample 0410b. The dashed lines show the fits of the broad PL bands using Eq. (4).

bands are caused by three different defects. Therefore, neither YL_{Be} nor RL_{Be} originates from the deep polaronic acceptor state of the Be_{Ga} acceptor since the shallow state of this acceptor is responsible for the UVL_{Be} band [7]. The three Be-related PL bands will be analyzed in detail in Sec. III C-III E. In the following section we present the results of theoretical calculations in which formation energies and transition levels for a number of Be-related defects are calculated, and the pool of candidates for the defects responsible for the above PL bands is narrowed.

B. Theoretical search for the PL bands candidates

At the initial stage of defect identification, HSE calculations for common Be-related point defects, including Be-containing complexes were performed using smaller 128 atom hexagonal GaN supercells. We have analyzed Be atoms substituting for gallium (Be_{Ga}), nitrogen (Be_N), the interstitial Be (Be_i), as well as their donor-acceptor combinations with each other and common point defects, such as oxygen donor (O_N), V_N and gallium vacancy (V_{Ga}). Optical properties of the promising candidates were then computed using 300 atoms supercells.

Fig. 3 shows the summary of the Be-related defect energetics in GaN. The Be_{Ga} is an acceptor, with HSE calculations predicting both shallow and deep polaronic acceptor states.

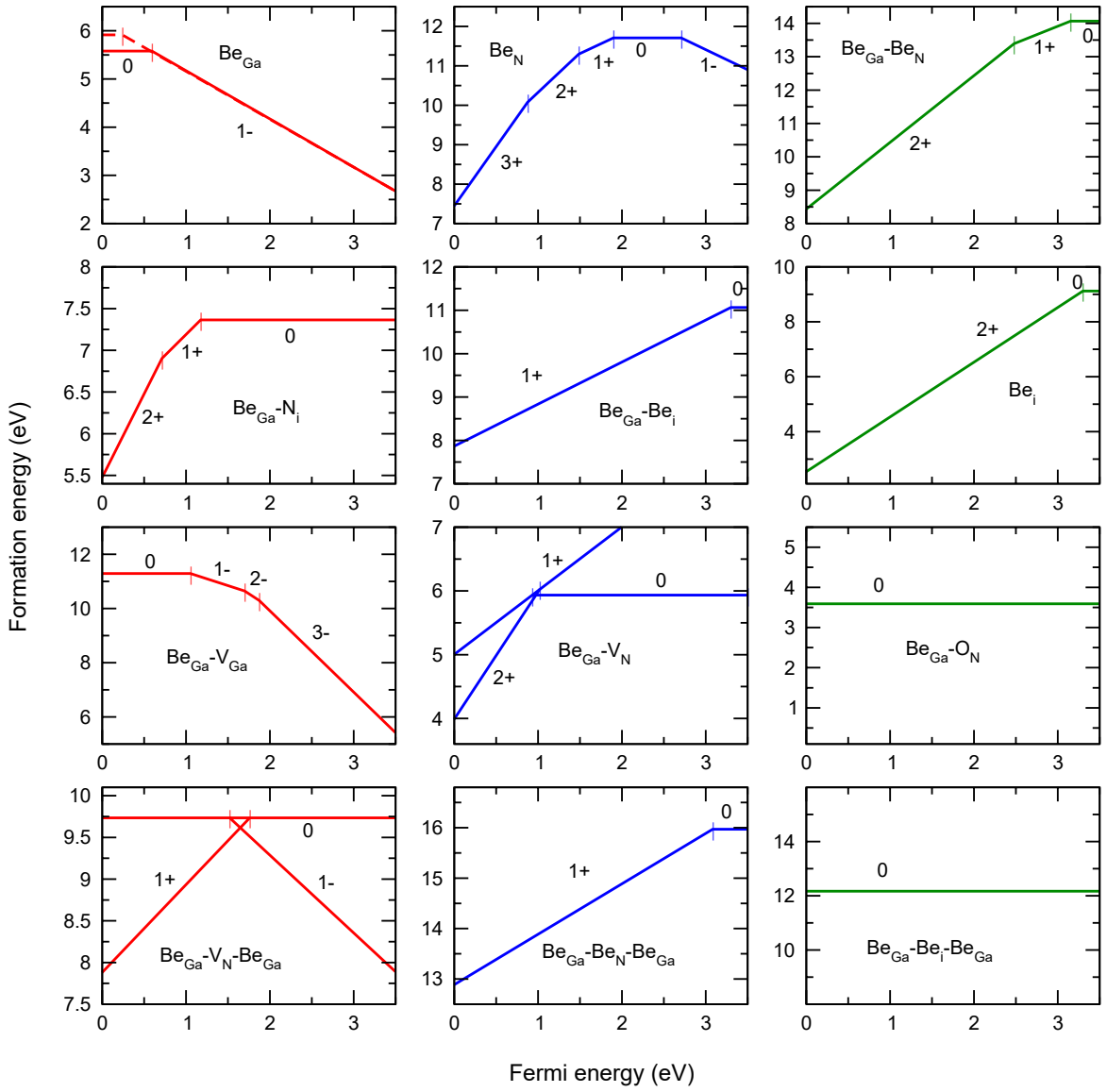

FIG. 3. (Color online) Formation energies (in N-rich growth regime), charge states, and transition levels of Be-related defects in GaN.

The polaronic ground state of the hole localized on a neutral Be_{Ga} acceptor (shown with a solid line in Fig. 3) has been analyzed in detail recently [7] and is not revealed in PL experiments. On the other hand, the shallow state of the neutral Be_{Ga} acceptor (shown with a dashed line in Fig. 3) is suggested to be responsible for the UVL_{Be} band observed in this work and is addressed below in Sec. III C. Both states compete for the photogenerated holes, and previous calculations show [7] that the delocalized shallow state captures the hole

significantly more efficiently. This leads to the bright UVL_{Be} originating from the shallow state of Be_{Ga}, and no observable PL from the polaronic state. The Be_N has higher a formation energy and displays a series of deep donor transition levels and a very deep $0/-$ acceptor level. Coulomb attraction can lead to the formation of a stable Be_{Ga}-Be_N complex, which is a deep donor, although it has high formation energy, especially in n-type material. Interstitial Be_i is a shallow double donor with a relatively low formation energy in p-type GaN, suggesting that self-compensation of Be_{Ga} acceptor by Be interstitials is likely [31].

Overall, most Be complexes appear to be detrimental to the incorporation of the Be_{Ga} acceptors. For example, the Be_{Ga} binds into donor complexes with nitrogen, beryllium, and gallium interstitials, with the Be_{Ga}-N_i having relatively low formation energy. The Be_{Ga}-Ga_i complex is found to be unstable, with gallium interstitial atom pushing beryllium out of the gallium site, forming a beryllium interstitial. The Be_i also can form a shallow donor complex with the Be_{Ga} acceptor.

The Be_{Ga} acceptor can form stable complexes with both gallium and nitrogen vacancies. The Be_{Ga} complex with the V_{Ga}, which is a weakly bound deep acceptor, is unstable in n-type material. The formation energies of the Be_{Ga}-V_{Ga} complex are also high, therefore it is not expected to form in significant quantities. The next nearest neighbor complex Be_N-V_{Ga} is found to be unstable: upon relaxation, the Be atom moves into the V_{Ga}, forming a Be_{Ga}-V_N complex. Similarly, the Be_i-V_{Ga} complex is unstable, with Be moving into the vacancy, forming the Be_{Ga} acceptor. The Be_{Ga}-V_N complex forms a negative-U center [32] with a value of U of about -0.1 eV. The formation energy of this complex is relatively low even in N-rich growth conditions, as shown in Fig 3. The HSE calculations suggest that optical transitions via the $+/0$ level of this donor complex cause the RL_{Be} band (Sec. III E).

Oxygen is a common shallow donor in GaN, often responsible for n-type behavior of as-grown samples. It forms a stable complex with the Be_{Ga} acceptor. The Be_{Ga}-O_N complex was recently proposed as a defect responsible for the yellow band in bulk Be-doped GaN [18]. Note, that in the bulk samples the properties of the yellow band differ from the YL_{Be} observed in the MBE-grown samples studied in this paper. Nevertheless, our HSE calculations suggest that the Be_{Ga}-O_N complex is electrically neutral and does not have transition levels in the bandgap. Therefore, we do not reproduce the attribution of any yellow band to this complex.

A triplet complex Be_{Ga}-O_N-Be_{Ga} (not shown) is found to be very weakly bound, indicating

that the Be_{Ga}-O_N and Be_{Ga} do not interact. Most triplet complexes considered here were found to have significant formation energies, and therefore unlikely to form in large amounts. However, even defects with relatively high formation energy can be created in the right conditions. The formation energy is an indicator of the likelihood of forming a defect in equilibrium. The samples studied in this work were grown by MBE, which is a relatively cold and highly non-equilibrium growth. Therefore, if there is a Coulomb attraction between the complex constituents during growth, the complexes can form in concentrations significantly different from those predicted by equilibrium thermodynamics. One example of this could be Be_{Ga}-V_N-Be_{Ga} which is negatively charged in n-type material. It is a promising candidate for the defect responsible for the YL_{Be} band because the experiment suggests an efficient capture of the photogenerated holes by the YL_{Be} defect. This behavior is expected for a negatively charged acceptor, such as Be_{Ga}-V_N-Be_{Ga}. The only other defect with such property is the Be_{Ga}-V_{Ga} complex, discussed above. However, calculations suggest that it is unstable in n-type material, where the YL_{Be} band is strong. In contrast, the Be_{Ga}-V_N-Be_{Ga} complex has binding energies of 1.5-1.9 eV and 0.8 eV in p-type and n-type materials, respectively. Although the latter may indicate a relatively weakly bound complex, there is likely a significantly larger barrier for the complex dissociation. The complex can be formed during the sample growth due to the Coulomb interaction between a positive donor Be_{Ga}-V_N and a negative acceptor Be_{Ga}. After the sample cooling, subsequent dissociation of the complex involves additional migration barriers for Be in GaN. The Be_{Ga}-V_N-Be_{Ga} complex is a negative-U center with a value of U of -0.24 eV. The YL_{Be} band can be attributed to this complex, as described in Sec. III D. The energies of calculated transition levels with respect to the VBM and the complex binding energies are summarized in Table II.

C. Ultraviolet band

The UVL_{Be} band was observed in half of the samples with the spectra dominated by the YL_{Be} (as in Fig. 1 for sample 0408b) and in half of the samples with the strong GL2 band (as in Fig. 4 for sample 0418a).

The NBE emission is dominated by the donor bound exciton (DBE) peak at 3.478 eV [33]. On the high-energy side of the DBE peak, the free exciton (FE) peak appears as a shoulder at 3.484 eV (better resolved at $T = 50$ K). It is followed by the UVL_{Be} band with

TABLE II. HSE calculated transition levels of Be-related defects. Binding energies of Be complexes are given for the three values of the Fermi level corresponding to the p-type, semi-insulating, and n-type materials. Binding energies of triplet complexes are computed with respect to dissociating a triplet into Be_{Ga} and a remaining doublet, i.e. Be_{Ga}-V_N, Be_{Ga}-Be_N, and Be_{Ga}-Be_i.

Defect	q_1/q_2	Transition energy (eV)	Binding energy (eV)		
			E_F ∼VBM	E_F ∼midgap	E_F ∼CBM
Be_{Ga}	$0/-$ (shallow)	< 0.2			
	$0/-$ (polaronic)	0.58			
Be_N	$3+/2+$	0.88			
	$2+/+$	1.49			
	$+/0$	1.90			
	$0/-$	2.71			
Be_{Ga}-Be_N	$2+/+$	2.48	4.7	4.1	0
	$+/0$	3.15			
Be_{Ga}-N_i	$2+/+$	0.71	0	1.9	0.2
	$+/0$	1.17			
Be_{Ga}-Be_i	$+/0$	> 3.3	1.0	1.5	1.5
Be_i	$2+/+$	> 3.3			
	$+/0$	> 3.3			
Be_{Ga}-V_{Ga}	$0/-$	1.05	0.5	0	−1.6
	$-/2-$	1.70			
	$2-/3-$	1.90			
Be_{Ga}-V_N	$2+/+$	1.02	1.9	1.4	1.4
	$+/0$	0.93			
Be_{Ga}-O_N	-	-	1.8	1.8	1.8
Be_{Ga}-V_N-Be_{Ga}	$+/0$	1.76	1.5	0.8	0.8
	$0/-$	1.52			
Be_{Ga}-Be_N-Be_{Ga}	$+/0$	3.10	1.3	1.8	0.8
Be_{Ga}-Be_i-Be_{Ga}	-	-	0.7	1.1	1.0

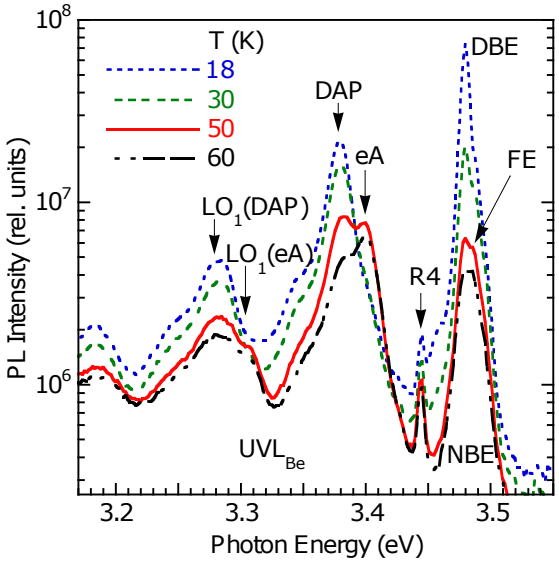

FIG. 4. (Color online) The high-energy part of the PL spectrum of sample 0418a measured at P_{exc} = 0.13 W/cm^2. At 3.444 eV, the fourth Raman line R4 from the He-Cd laser (3.814 eV) appears due to the interaction with the 92 meV bulk LO phonon mode. The ZPL of the DAP transition of the $\mathrm{UVL_{Be}}$ band peaks at 3.375 eV with its first LO phonon replica situated 92 meV further. The transitions from the conduction band to the acceptor (eA) replace the DAP transitions at temperatures above 50 K.

the ZPL at 3.375 eV and two phonon replicas separated by the bulk LO phonon energy of 92 meV. This band is identified as the DAP transition between shallow donors and the 0/− level of the $\mathrm{Be_{Ga}}$ acceptor (at low temperatures) [7]. The shape of the band suggests the Huang-Rhys factor of 0.2, typical for shallow acceptors [33]. The QEs of the $\mathrm{UVL_{Be}}$ band in different samples are presented in Table. I. The ZPL blue shifts by 6 meV with increasing excitation intensity P_{exc} from 10^{-5} to 0.1 W/cm^2 at low temperature. The shift agrees with the DAP origin of the transition. As temperature rises, the shallow donors ($\mathrm{O_N}$ and $\mathrm{Si_{Ga}}$) become ionized, and the DAP transitions transform into the eA transitions (from the conduction band to the same acceptor level). As a result, the DAP band is gradually replaced with the identical eA band, shifted by the donor ionization energy (about 20 meV) [33], with the ZPL at 3.395 eV. The eA transitions are best resolved above 50 K. Taking into account the FE binding energy ($\sim$ 26 meV) [34], the position of the 0/− transition level of the $\mathrm{Be_{Ga}}$ acceptor is estimated to be 113 ± 5 meV [7]. This makes $\mathrm{Be_{Ga}}$ a dopant with the lowest acceptor level in GaN observed to date.

The dependence of the UVL_{Be} intensity on temperature under different excitation intensities is shown in Fig. 5. The PL intensity does not change significantly at low temperatures and decreases exponentially above ~ 50 K. The temperature above which the decrease begins is tunable by excitation intensity and shifts to lower temperatures for lower excitation intensities. Such temperature behavior is similar to that of UVL_{Mg}, BL_{Zn}, and YL1 bands in high-resistivity GaN, related to the Mg_{Ga} [2], Zn_{Ga} [35], and C_N [24] acceptors, respectively. The temperature dependence of PL intensity is traditionally fitted with the following expression [33]

$$I(T) = \frac{I(0)}{1 + C \exp\left(-\frac{E_A}{kT}\right)}, \tag{1}$$

where $I(0)$ is the intensity in the low-temperature limit, E_A is the activation energy of the thermal quenching, and C is the pre-exponential factor. As an example, the dependence for $P_{exc} = 0.016$ W/cm^2 in Fig. 5 is fitted with Eq. (1) with parameters $C = 3.4 \times 10^5$ and $E_A = 70$ meV. However, the conventional interpretation of this formula, as the thermal emission of holes from the defect level at E_A above the VBM and re-capture of these holes by nonradiative defects (the Schön-Klasens mechanism), fails to explain the shift of the exponential decrease region to higher temperatures when P_{exc} increases [36]. The abrupt and tunable quenching (ATQ) model can be utilized to explain such discrepancy, as described

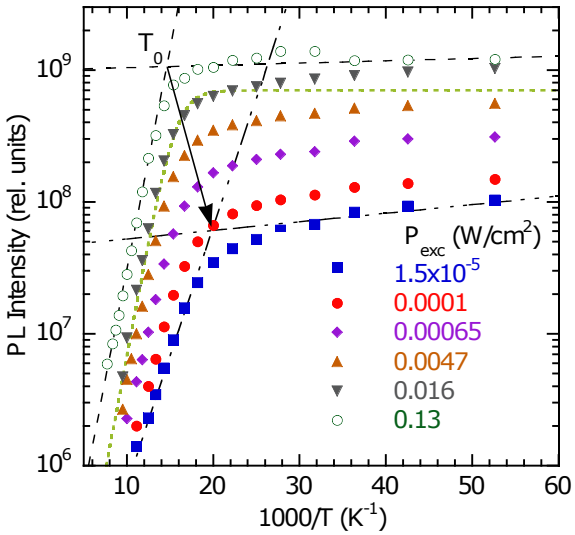

FIG. 5. (Color online) Temperature dependences of the UVL_{Be} peak intensity divided by P_{exc} for sample 0414b at various excitation intensities. The low-temperature region and the exponential drop of the PL intensity linearly extrapolated in Arrhenius coordinates define the position of T_0.

below.

The ATQ model introduced in Ref. [35] provides a plausible explanation for the UVL_{Be} quenching. It involves an inverse population of defect levels with charge carriers at low temperatures due to preferential capture of photogenerated holes by radiative acceptors and electrons by nonradiative donors. Let T_0 be the critical temperature defined as the intersection between extrapolated low-temperature dependence and the exponential drop in the Arrhenius plot (Fig. 5). At low temperatures in the steady-state conditions, almost all nonradiative donors become populated with photogenerated electrons. The fast capture of photogenerated holes by acceptors is followed by radiative transitions from the shallow donors or the conduction band to the acceptor. At T_0 the concentrations of thermally emitted (proportional to $\exp(-E_A/kT)$) and photogenerated holes become comparable. These holes, re-captured by the nonradiative donors, break the bottleneck in the nonradiative recombination channel and quickly depopulate the nonradiative donors within the very narrow temperature range. The limiting concentration of free holes that unlocks the nonradiative channel is proportional to the electron-hole generation rate G, which results in the tunability of T_0 [35, 36]. In this case, the T_0 depends on G as [35]

$$T_0 = \frac{E_A}{k \ln\left(QT_0^{3/2}/G\right)}, \tag{2}$$

with

$$Q = C_{pA}\left(\frac{1}{\eta_0} - 1\right)(N_A - N_D)\frac{N_{v1}}{g}, \tag{3}$$

where C_{pA} is the hole-capture coefficient for the acceptor, η_0 is the absolute QE of the UVL_{Be} band, N_A and N_D are the acceptor and shallow donor concentrations, g is the degeneracy of the acceptor level, and N_{v1} is the effective density of states in the valence band at $T = 1$ K. The G is calculated using absorption coefficient ($\alpha = 10^5$ cm^{-1} for GaN at 325 nm [37]) as $G = \alpha P_{\text{exc}}/\hbar\omega_{\text{exc}}$ under the assumption that the incident photons are absorbed uniformly within the layer of thickness α^{-1}. Note that the quenching of the UVL_{Be} band is tunable but does not look abrupt. As numerical calculations suggest, the initial abrupt drop of PL is obscured by the following exponential decrease with the activation energy E_A [36]. This is typical for shallow acceptors when their concentration is larger than the concentration of shallow donors but smaller than the total concentration of donors (radiative and nonradiative) [36].

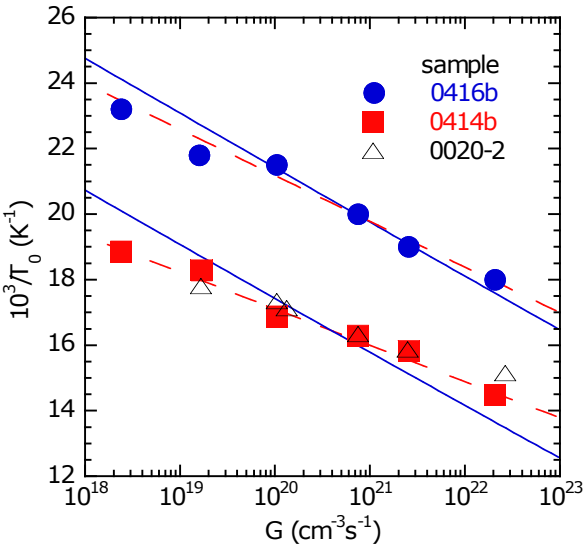

FIG. 6. (Color online) Dependence of the critical temperature T_0 on the electron-hole generation rate G for the UVL_{Be} band in GaN:Be (samples 0416b, 04014b, and 0020-2, all semi-insulating). The fits using Eqs. (2) and (3) with the fixed $E_A = 113$ meV are shown with the solid lines and reveal $Q = 5 \times 10^{29}$ and 2×10^{27} $cm^{-3}s^{-1}K^{-3/2}$ for samples 0416b and 0414b, respectively.

The $T_0(G)$ dependence for the UVL_{Be} band in three samples is plotted in Fig. 6. If we consider both E_A and Q as fitting parameters (dashed lines in Fig. 6), we obtain $E_A = 135$ meV and $Q = 8 \times 10^{31}$ $cm^{-3}s^{-1}K^{-3/2}$ (sample 0416b) and $E_A = 170$ meV and $Q = 1 \times 10^{32}$ $cm^{-3}s^{-1}K^{-3/2}$ (sample 0414b), where E_A disagrees with the PL spectroscopy data [7], and Q results in a very large capture coefficient C_{pA}. Indeed, by taking QE for the UVL_{Be} band and the total concentration of Be obtained from SIMS analysis (e.g., $\eta_0 = 0.0012$ and $N_A - N_D < 10^{18}$ cm^{-3} for sample 0416b), we get C_{pA} from Eq. (3) larger than 3×10^{-5} and 6×10^{-5} cm^3/s for samples 0414b and 0416b, respectively. Nevertheless, the model is still valid if we fix E_A to 113 meV (known from DAP to eA transformation) and make $C_{pA} = 10^{-6}$ cm^3/s, which is the crude estimate accurate to plus-minus order of magnitude. The fit accuracy somewhat worsens (solid lines in Fig. 6), but the parameter Q takes reasonable values (2×10^{27} and 5×10^{29} $cm^{-3}s^{-1}K^{-3/2}$ for samples 0414b and 0416b) that yield $N_A - N_D = 6 \times 10^{15}$ and 4×10^{17} cm^{-3} for samples 0414b and 0416b. Note that C_{pA} and $(N_A - N_D)$ appear as product in Eq. (3) and cannot be determined independently. Nevertheless, it can be concluded that $C_{pA} > 4 \times 10^{-7}$ cm^3/s (otherwise, $N_A - N_D >$ [Be] for sample 0416b), and the concentration of the Be_{Ga} acceptors responsible for the UVL_{Be} band

is much lower than the concentration of defects responsible for the YL_{Be} band in selected samples (Table I). The weaker $T_0(G)$ dependence than expected for $E_A = 113$ meV could be explained by the presence of the depletion region near the sample surface [36]. Hence, the ATQ model explains recombination kinetics in the bulk of the samples, but the experimental dependences are distorted by the surface effects.

Detailed HSE calculations of optical properties of the Be_{Ga} acceptor were presented in Ref. [7]. The HSE calculations predict that the Be_{Ga} is a dual-nature acceptor, possessing both deep and shallow acceptor states. The deep state is obtained by the relaxation of the defect lattice geometry from the starting point where the Be-N bond is extended by about

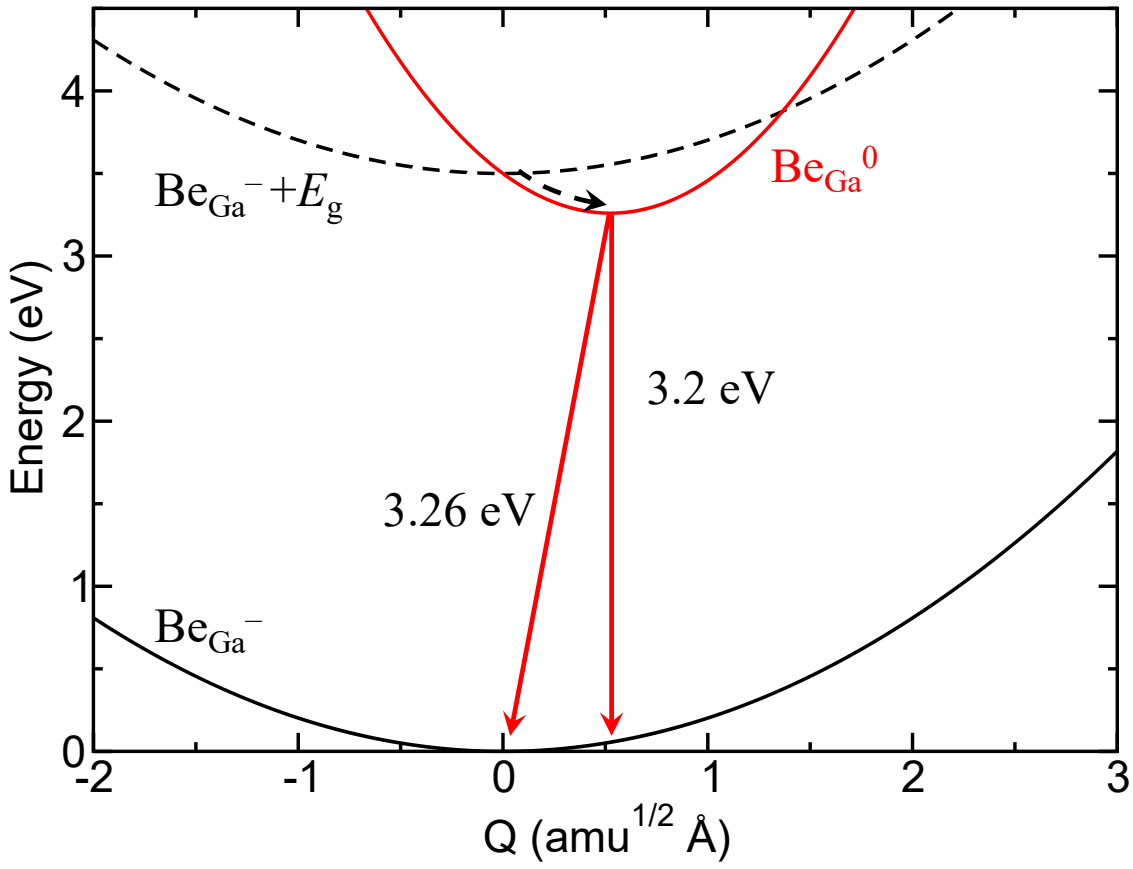

FIG. 7. (Color online) Configuration coordinate diagram for the shallow state of the Be_{Ga} acceptor. In the ground state, acceptor is negatively charged. The photogenerated hole is efficiently captured (dashed arrow) to the shallow state of the acceptor, with subsequent radiative transitions calculated to have the PL maximum at 3.2 eV and the ZPL at 3.26 eV.

0.7 Å from its equilibrium value. The shallow state can be obtained by relaxing the defect structure starting from the ideal GaN lattice. The deep state is a small polaron with a transition level calculated at 0.58 eV above the VBM. The deep state of the Be_{Ga} has not been observed experimentally, likely due to the low hole capture coefficient of the polaronic state (about 2 orders of magnitude lower than that of the shallow state). The shallow state shown in Fig. 7 is predicted to have a transition level at about 0.2 eV, a value overestimated by about 0.1 eV due to the supercell approach. Upon photoexcitation, the shallow state of the Be_{Ga} acceptor efficiently captures a hole, with the capture coefficient estimated between 10^{-6} and 10^{-5} cm^3/s [7], due to the absence of the potential barrier for this process (the dashed arrow in Fig. 7). Optical transitions via the shallow acceptor state of the Be_{Ga} are predicted at 3.26 eV (ZPL) and 3.20 eV (PL band maximum) in good agreement with the experiment. The calculated Huang-Rhys factor is 2.8, a value also overestimated due to the difficulties in describing a shallow defect state within the supercell approach. Both experimental data and theoretical results indicate that the UVL_{Be} band in Be-doped GaN samples originates from the shallow state of Be_{Ga} acceptor.

D. Yellow band

Fig. 8 shows the broad YL_{Be} band with a maximum at 2.13 eV, which dominates the lower-energy portion of the spectrum in the majority of the GaN:Be samples. The band's shape can be fitted with the formula derived from the configuration coordinate model [21]

$$I(\hbar\omega) = I_0 \exp\left\{-2S_e\left(\sqrt{\frac{E_0-\hbar\omega}{E_0-\hbar\omega_{\max}}}-1\right)^2\right\}, \quad (4)$$

where $\hbar\omega_{\max}$ is the position of the band maximum, S_e is the Huang-Rhys factor and E_0 is a parameter with the magnitude close to the ZPL energy. A reasonably good fit can be obtained with $E_0 = 3.3$ eV, $\hbar\omega_{\max} = 2.13$ eV and $S_e = 27$. The band blue-shifts by less than 20 meV with increasing P_{exc} from 0.01 to 100 W/cm^2. It also significantly differs from the YL1 band attributed to C_N defect that has the same maximum position. The shapes of the two bands are compared in Fig. 8, where the spectrum of the YL1 band is taken from the C-doped MOCVD GaN sample, details on which can be found in Ref. [24]. The temperature dependence of the intensity demonstrates even greater dissimilarity between the YL1 and YL_{Be} bands.

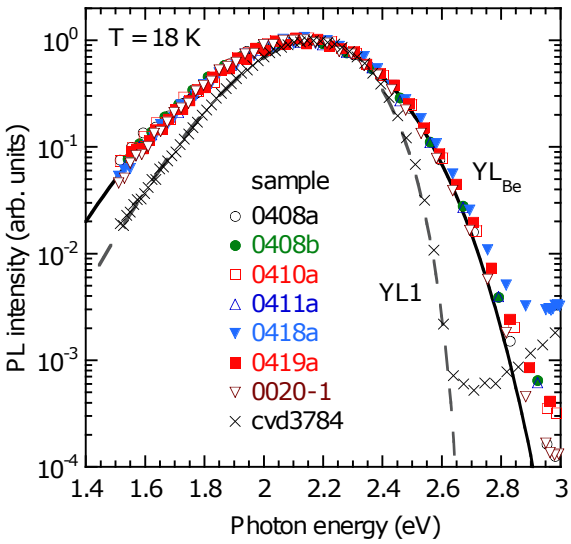

FIG. 8. (Color online) Normalized shapes of the YL_{Be} band in GaN:Be samples compared to the YL1 band from the MOCVD-grown GaN:C sample cvd3784. The YL1 band is attributed to the C_N defect [24]. The solid and dashed lines are calculated using Eq. (4) with the following parameters: $E_0 = 2.67$ eV, $\hbar\omega_{\max} = 2.17$ eV and $S_e = 7.6$ (the YL1 band) and $E_0 = 3.3$ eV, $\hbar\omega_{\max} = 2.13$ eV and $S_e = 27$ (the YL_{Be} band).

The quenching of the YL_{Be} intensity with temperature occurs in two steps: a relatively small stepwise decrease is observed at about 100 K, and the second (usually abrupt) quenching begins at about 200 K. In semi-insulating samples, both quenching steps are tunable, and the second quenching is abrupt, the behavior similar to that in semi-insulating GaN doped with Zn [38]. The magnitude of the first step is sample-dependent. In n-type GaN:Be sample, the quenching of the YL_{Be} band is neither tunable nor abrupt, which is typical for n-type GaN [35]. Below, the temperature dependences of the YL_{Be} band in n-type and semi-insulating GaN:Be samples are presented in two separate sections.

1. *n-type GaN:Be*

Only one of the studied samples (0020-1) demonstrated PL behavior typical for a conductive n-type GaN. In particular, the PL decay of the YL_{Be} was nearly exponential at $T > 100$ K, and the PL quenching occurred by the Schön-Klasens mechanism. The Hall effect measurements at room temperature confirmed n-type conductivity with $n = 6 \times 10^{17}$ cm^{-3}. When decay of PL intensity after a laser pulse in TRPL measurements is close to

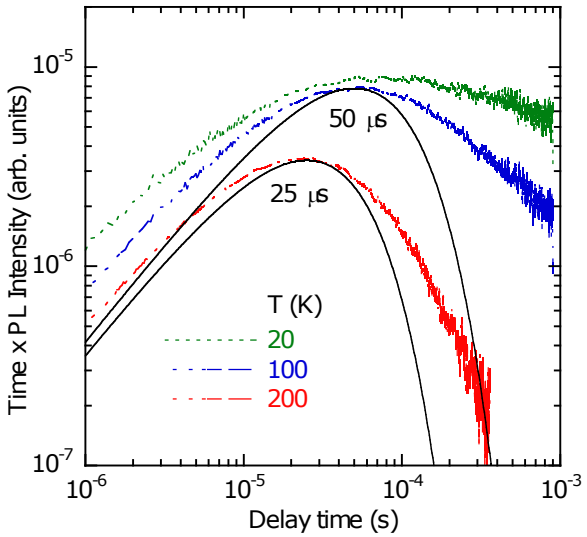

FIG. 9. (Color online) The product of delay time and PL intensity decay after the excitation laser pulse for the YL_{Be} band in n-type sample 0020-1. The solid lines are the dependences of the form $te^{-t/\tau}$. The maximum of the dependence corresponds to the effective lifetime of the band at a given temperature. At temperatures below 50 K the method is inconclusive. With increasing temperature, lifetime decreases from 50 μs at 100 K to 25 μs at 200 K. The raw data was filtered using Wiener optimal filter.

exponential (but not exactly exponential), the PL lifetime can be found as the time corresponding to a maximum in the $t \cdot I^{PL}(t)$ dependence [39]. Examples for the YL_{Be} band in sample 0020-1 are shown in Fig. 9. The effective PL lifetime is 50 μs at $T = 100$ K and decreases to 25 μs at $T = 200$ K. The decrease in lifetime τ is expected due to the thermal excitation of electrons from the shallow donors to the conduction band according to relation $\tau = (nC_{nA})^{-1}$, where n is the concentration of free electrons. With $n = 4 \times 10^{17}$ cm^{-3} at $T = 200$ K, we estimate that $C_{nA} = 10^{-13}$ cm^{-3}s^{-1} for the defect responsible for the YL_{Be} band. This value is close to the electron-capture coefficient for the major acceptors in undoped GaN: 3.2×10^{-13}, 0.68×10^{-13}, and 0.11×10^{-13} cm^{-3}s^{-1} for the Mg_{Ga}, Zn_{Ga}, and C_N acceptors [40].

The intensity of the YL_{Be} band in n-type GaN:Be (sample 0020-1) is nearly independent of temperature up to $\sim$ 150 K (the first step is very small). At higher temperatures, it decreases with the activation energy $E_A = 0.3$ eV (Fig. 10). The characteristic temperature at which the quenching begins is not tunable by excitation intensity and can be meaningfully

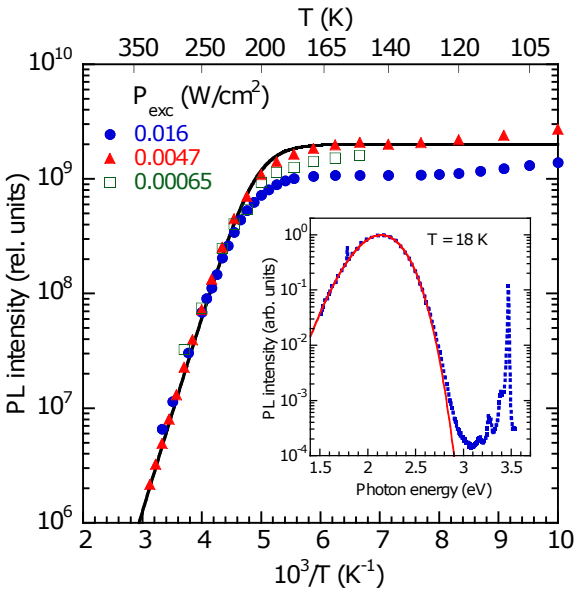

FIG. 10. (Color online) Temperature dependences of the peak PL intensity of the YL_{Be} band in the n-type sample 0020-1 at different P_{exc}. The data for $P_{exc} = 0.0047$ W/cm^2 are fitted using Eqs . (1) and (5) with the following parameters: $E_A = 0.3$ eV, $C_{pA} = 4.0\times10^{-7}$ cm^{-3}s^{-1}, $N_{v1} = 3.5\times10^{15}$ cm^{-3}, $\tau = 25$ μs, and $\eta_0 = 0.25$. The inset shows PL spectrum at $T = 18$ K (dotted line) and calculated shape using Eq. (4) with the following parameters: $E_0 = 3.3$ eV, $\hbar\omega_{max} = 2.14$ eV and $S_e = 27$.

fitted with Eq. (1), provided that the pre-exponential factor is given by [35]

$$C = (1-\eta_0)\tau C_{pA} N_{v1} T^{3/2}/g. \tag{5}$$

Here, η_0 is the QE of the PL band, τ is the characteristic lifetime of the PL before quenching, C_{pA} is the hole-capture coefficient, g the degeneracy factor, and N_{v1} is the effective density of states at $T = 1$ K. The PL lifetime of the YL_{Be} band was determined from the TRPL measurements to be $\tau = 25$ μs at $T = 200$ K. From Eq. (5), with $\eta_0 = 0.25$, and $N_{v1} = 3.5 \times 10^{15}$ cm^{-3}, the hole capture coefficient can be found as $C_{pA} = 4.0 \times 10^{-7}$ cm^3/s and $E_A = 0.30$ eV. A relatively large value of the hole capture coefficient suggests that the defect responsible for the YL_{Be} band is likely an acceptor which is negatively charged in the n-type sample.

2. Semi-insulating GaN:Be

For all semi-insulating GaN:Be samples, the YL_{Be} band abruptly quenched at temperatures lower than 200 K, and the attempts to fit the temperature dependence of the PL intensity with Eq. (1) resulted in unreasonably large sample-dependent activation energies (ranging from 600 to 1300 meV) and pre-exponential factors C (from 10^{32} to 4×10^{39}). Examples of such dependences for one of the samples are shown in Fig. 11.

Similar to the UVL_{Be}, the exponential PL intensity drop starts at higher temperatures as the excitation intensity increases. Such temperature behavior of the PL is typical for semi-insulating samples [35]. This is another example where the ATQ model explains recombination kinetics and yields at least rough estimates of the parameters. It should be emphasized that in this case, fitting the temperature dependences of the PL intensity with Eq. (1) yields incorrect activation energies. For example, in Fig. 11 the temperature dependence is fitted using Eq. (1) with the following parameters: $E_A = 1030$ meV and $C = 1 \times 10^{32}$, 1×10^{36}, and 4×10^{39} in order of decreasing P_{exc}.

The $T_0(G)$ dependence shown in Fig. 12, can be fitted with Eqs. (2) and (3), as in the case of the UVL_{Be}. Using $E_A = 0.30$ eV and $C_{pA} = 4 \times 10^{-7}$ $\text{cm}^{-3}\text{s}^{-1}$, known from the n-type sample, and the QE of the YL_{Be} band determined from a comparison of the integrated

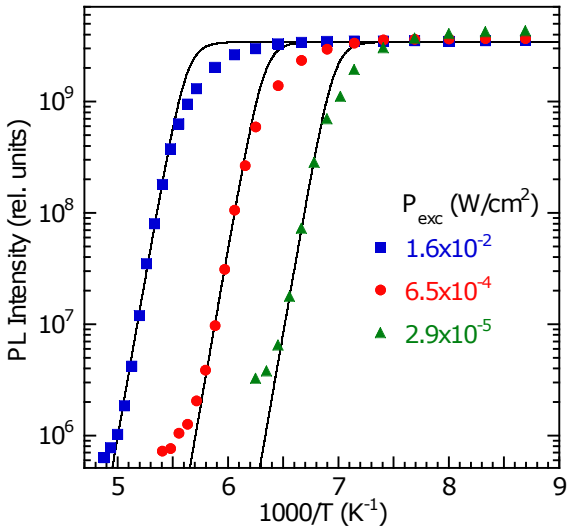

FIG. 11. (Color online) The temperature dependences of the peak YL_{Be} intensity in the semi-insulating GaN:Be (sample 0408a). Excitation intensity P_{exc} is varied in the range $2.9 \times 10^{-5} - 1.6 \times 10^{-2}$ W/cm^2.

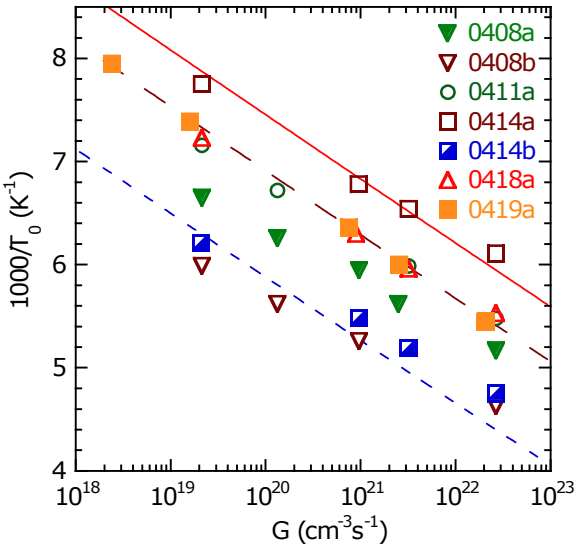

FIG. 12. (Color online) Dependence of the critical temperature T_0 on the electron-hole pair generation rate G for the YL_{Be} band in semi-insulating GaN:Be samples. In the examples of fits with Eq. (2) shown with lines, parameters $C_{pA} = 4 \times 10^{-7}$ cm^{-3}s^{-1}, $E_A = 0.30$ eV, and $N_{v1} = 3.5 \times 10^{15}$ cm^{-3} are taken from the n-type sample analysis, and the obtained values of $N_A - N_D$ are given in Table I.

YL_{Be} intensity with calibrated GaN samples, the value of $N_A - N_D$ can be obtained. For all the samples analyzed in such a way, it is smaller than the total concentration of Be atoms (Table I). Note that the obtained values are rough estimates because the quantum efficiency is usually found with the accuracy of plus-minus half an order of magnitude [41]. This shows that the ATQ model is valid and is consistent with the data obtained from the n-type sample.

The identification of the defect responsible for the YL_{Be} is difficult. There are several restrictions imposed on this identification by the experimental data: a) The defect is likely an acceptor with a transition level at 0.3 eV above the VBM rather than a donor. This follows from a high C_{pA} and low C_{nA}; b) The defect is Be-related, as the YL_{Be} band is only observed in samples doped with Be. It is unlikely to be related to other impurities, common in GaN, but it could be a complex of Be with a native defect or a common impurity; c) the YL_{Be} band is due to the transition of an electron from the conduction band (or a shallow donor) to an acceptor level at 0.3 eV above the VBM, and it is not a radiative capture of a hole by a level 0.3 eV below the CBM. This type of transition is supported by the fact that

the bright YL_{Be} band is observed in the n-type sample, where the PL lifetime for this band is ~ 50 μs at 20 K. If this PL were due to the radiative capture of holes from the valence band, these slow transitions could not compete with fast nonradiative capture of holes by other defects, such as the Mg_{Ga} acceptor, which is present in GaN as contaminant. Finally, the YL_{Be} band in the studied MBE GaN:Be samples differs from the yellow band in bulk GaN:Be. In the latter, the yellow luminescence is very strong at room temperature [42] and its quenching begins at $T > 500$ K [19].

Among the computed Be-related defects and complexes (Be_i, Be_N, Be_{Ga}-O_N, Be_{Ga}-V_N-Be_{Ga}, V_{Ga}-Be_i, Be_{Ga}-O_N-Be_{Ga}, Be_{Ga}-Be_N-Be_{Ga}, Be_{Ga}-Be_i-Be_{Ga}, Be_{Ga}-N_i, V_{Ga}-Be_N, Be_{Ga}-Ga_i, V_{Ga}-Be_{Ga}), none exhibit an acceptor level at around 0.3 eV. Note that we also did not reproduce the previously suggested attribution of the YL_{Be} band to the Be_{Ga}-O_N complex [18]. Our calculations show that this complex does not have any transition levels in the bandgap. The polaronic $+/0$ transition level of the Be_{Ga}-O_N complex is found below the VBM for several HSE functional parametrizations, including that reproducing the bulk GaN bandgap. Attribution of the YL_{Be} to the Be_{Ga}-O_N complex also contradicts one of the above experimental results, i.e., the high C_{pA} and low C_{nA} for the YL_{Be} defect, indicating that it is unlikely to be a donor.

A possible explanation for the nature of the YL_{Be} band is the Be_{Ga}-V_N-Be_{Ga} complex. It is the only stable defect that is negatively charged for the Fermi energy above about 1.5 eV. This complex can help explain the YL_{Be} band under the assumption of the existence of an excited state for the hole around 0.3 eV above the VBM. A configuration coordinate diagram, which is a combination of the HSE calculations and experimental data, is presented in Fig. 13.

The YL_{Be} band is not observed in samples with a strong GL2 band. This is likely because the Fermi level in these samples is below the $0/-$ level of the Be_{Ga}-V_N-Be_{Ga} complex, computed at 1.5 eV. In this case, the defect is in the positive charge state, as shown in Fig. 3 (negative-U center), and the excited state for the hole does not form. In semi-insulating or n-type samples, the Be_{Ga}-V_N-Be_{Ga} complex is in the negative charge state (lower adiabatic potential in Fig. 13). The photogenerated electron-hole pair raises this adiabatic potential by the energy E_g (upper dashed potential labeled Be_{Ga}-V_N-$Be_{Ga}^{-} + E_g$). From this state, a hole can be captured to the defect ground state (the potential labeled Be_{Ga}-V_N-Be_{Ga}^{0}) as shown with a dashed arrow. This capture occurs without any appreciable

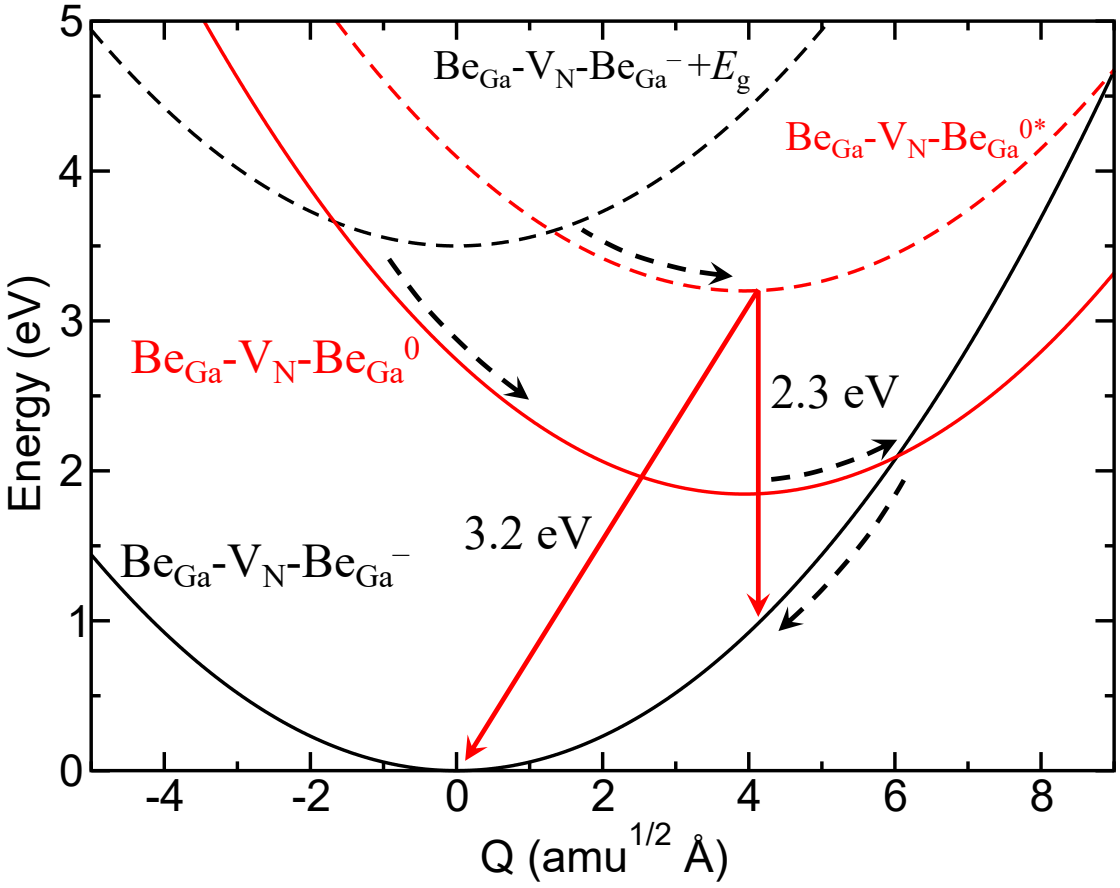

FIG. 13. (Color online) Configuration coordinate diagram for the Be_{Ga}-V_N-Be_{Ga} complex. In semi-insulating or n-type samples, the defect is negatively charged. The photogenerated hole can be captured (dashed arrows) either to the ground state of the hole, i.e., the neutral state Be_{Ga}-V_N-Be_{Ga}^0, or to the excited state Be_{Ga}-V_N-Be_{Ga}^{0*}. The transition via the ground 0/− level of the Be_{Ga}-V_N-Be_{Ga} complex is predicted to be nonradiative. The transition where the electron recombines with the hole in the excited state is radiative with the PL maximum of 2.3 eV and ZPL of 3.2 eV.

potential barrier. The transition from the neutral state to the negative state, i.e., via the 0/− thermodynamic transition level, also exhibits a relatively low potential barrier of 0.25 eV, suggesting the mostly nonradiative nature of these transitions (all are shown with the dashed arrows). Experimental measurements suggest the existence of an excited state of the hole (the potential labeled Be_{Ga}-V_N-Be_{Ga}^{0*}), for which the hole capture is also efficient and without a barrier (shown with a dashed arrow). If the defect lattice structure for the excited

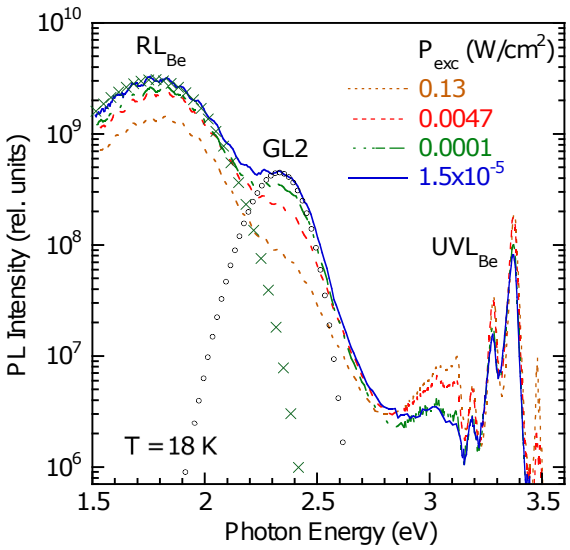

FIG. 14. (Color online) SSPL spectra from Be-doped GaN (sample 0416b) at $T = 18$ K and selected excitation intensities. The red, green, and ultraviolet luminescence bands are denoted as RL_{Be}, GL2 and UVL_{Be}, respectively. The shapes of the bands (shown with green crosses and black circles) were simulated with Eq. (4), where $E_0 = 2.7$ eV, $\hbar\omega_{max} = 1.77$ eV and $S_e = 20$ for the RL_{Be} and $E_0 = 2.85$ eV, $\hbar\omega_{max} = 2.33$ eV and $S_e = 26.5$ [21] for the GL2. We could not identify the feature in-between the GL2 and UVL_{Be} bands, and it was not reproduced among the samples.

state of the hole is similar to that of the ground state, an assumption made in Fig. 13, there is no nonradiative recombination route from this excited state to the negative ground state. As a result, only radiative transition from the excited state to the ground state is possible. Taking the ZPL of the YL_{Be} from the experiment to be 3.2 eV, HSE calculations yield a Franck-Condon shift [43] of 0.9 eV, placing the predicted PL maximum of the radiative transition at 2.3 eV, in a reasonable agreement with experiment.

E. Red band

In samples with strong YL_{Be}, the red band is very weak (Table I) and can be resolved only after the quenching of the YL_{Be} band, which makes its analysis and attribution difficult. The RL_{Be} is strong in several annealed samples where it overlaps with the green GL2 band. Fig. 14 shows typical SSPL spectra from the annealed sample 0416b. The RL_{Be} band has a maximum at 1.77 eV and Huang-Rhys factor 20 according to Eq. (4). The GL2 band with a

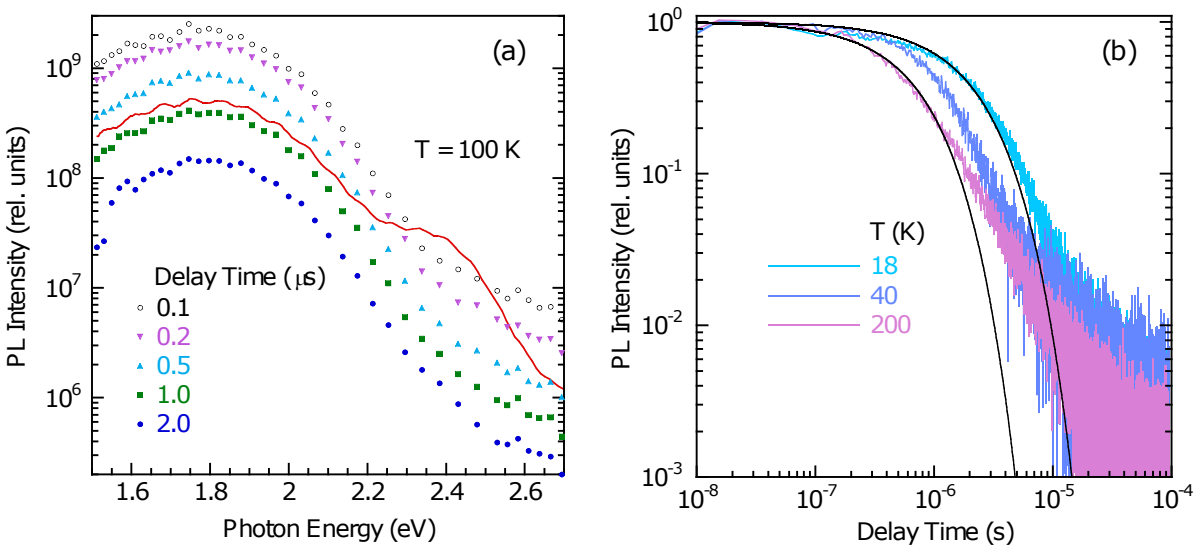

FIG. 15. (Color online) TRPL from sample 0416b. (a) The TRPL spectra at $T = 100$ K and selected time delays after the laser pulse. At longer time delays, the GL2 band with the characteristic lifetime of about 0.2 ms can be resolved (not shown). The SSPL spectrum at $P_{\rm exc} = 0.0047$ W/cm^2 is shown with the solid line for comparison. (b) Normalized decays at 1.8 eV at selected temperatures. The RL_{Be} band decays exponentially and can be traced up to about 0.1 ms. The thick solid lines are the exponents with lifetimes 0.7 and 2.1 μs.

maximum at 2.33 eV is attributed to the internal transitions via defect levels of the V_N [21]. Its shape is well known, and it completely quenches by the room temperature, revealing a broadened shape of the RL_{Be} band. To determine the parameters of the RL_{Be} band at low temperatures, the spectrum should be deconvoluted. The RL_{Be} was not saturated up to $P_{\rm exc} = 0.13$ W/cm^2. The peak intensity of the RL_{Be} band is independent of temperature up to 100 K and decreases by an order of magnitude by 300 K.

Analysis of TRPL, shown in Fig. 15, provides additional information about the RL_{Be} band. Its shape in SSPL and TRPL experiments is the same, which indicates that the broad red band is caused by one defect. The PL decay after the laser pulse at $T = 18$ K is exponential for both RL_{Be} and GL2 bands, with lifetimes about 2 μs (Fig. 15(b)) and 250 μs (not shown), respectively. The RL_{Be} lifetime decreases by a factor of 3 in the temperature range from 18 to 200 K (Fig. 15(b)).

The RL_{Be} band in the SSPL spectra can be confused with the RL1 [36], RL2 [44, 45] or RY3 [46] bands in undoped GaN with the maxima at 1.73 , 1.72, and 1.77 eV, respectively,

unless additional time-resolved and temperature measurements are taken. The RL1 band often appears in n-type GaN grown by HVPE and is attributed to the DAP transition. Unlike the RL_{Be}, the decay of the RL1 is nonexponential at low temperature and becomes exponential with $\tau \sim 1$ ms at $T = 100$ K. The RL2 band is observed in Ga-rich, semi-insulating GaN. It is caused by an internal transition from an excited state to the ground state of an unidentified defect and can be distinguished by the slow exponential decay after laser pulse [33]. Its lifetime decreases from 110 to 2 μs with increasing temperature from 15 to 100 K [45]. The RY3 band is found in undoped n-type GaN grown with HVPE and consists of two components, namely RL3 and YL3, both originating from the same defect [46]. A careful comparison of the properties of all these red bands in GaN shows that the RL_{Be} is a new, Be-related PL band.

HSE calculations suggest that the RL_{Be} band originates from the Be_{Ga}-V_N complex. The configuration coordinate diagram for this defect is shown in Fig. 16. Calculations predict this complex to be a deep donor, with the +/0 transition level at 0.95 eV above the VBM. When the Fermi level is above the +/0 level, the defect is neutral in the ground state (the lower potential in Fig. 16). An electron-hole pair is created by the above-bandgap photoexcitation, raising the energy of the system by the GaN bandgap of 3.5 eV (the dashed potential). Resonant excitation energy for this defect (3.42 eV) is close to the bandgap value. The photogenerated hole is captured by the Be_{Ga}-V_N complex without a barrier (the dashed arrow in Fig. 16), releasing the excess energy of 0.95 eV as phonons and converting the defect into positively charged. The nonradiative transition from the positive to the neutral charge state of the complex is hindered by a large potential barrier for this transition of about 1 eV (the + and 0 potentials intersect at $Q \sim 8.2$ amu$^{1/2}$Å, with the energy of 3.6 eV), making this defect radiative. The radiative transition is shown with a downward arrow, which causes a red band with a calculated maximum of 1.73 eV and ZPL of 2.55 eV, in good agreement with the experimental results. Note that from the experiment the RL_{Be} band is caused by an internal transition: from an excited state presumably located close to the conduction band to the deep ground state of the donor. The transition of electrons from the conduction band to the ground state is much less efficient and could contribute to the tail in the RL_{Be} decay shown in Fig. 15(b). Most likely, the excited state is a hydrogenic Coulomb state appearing below the CBM only when the donor is positively charged.

With the above attribution of the YL_{Be} and RL_{Be} bands to the Be_{Ga}-V_N-Be_{Ga} and Be_{Ga}-

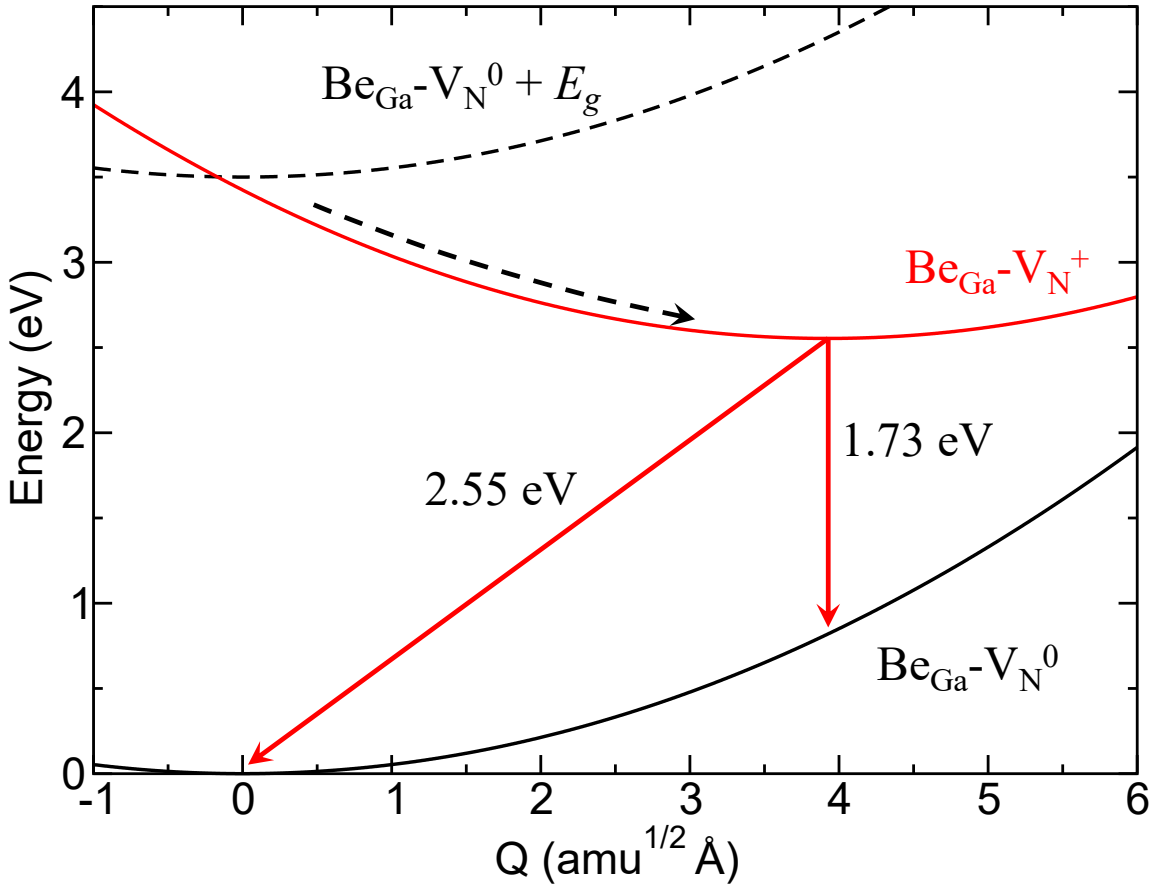

FIG. 16. (Color online) Configuration coordinate diagram for the Be_{Ga}-V_N complex. The photogenerated hole is captured by the Be_{Ga}-V_N defect, with subsequent radiative recombination with PL maximum calculated at 1.73 eV and ZPL at 2.55 eV.

V_N complexes, we can explain the regularities in the appearance of these bands in different samples mentioned in Sec. III A. The key point is the position of the Fermi level, which depends on the relative concentrations of defects and may sharply change across a sample. Figure 17 shows schematically transition levels of the defects studied in this work. The concentrations of the O_N, Be_{Ga}-V_N, V_N, Be_{Ga}, and Be_{Ga}-V_N-Be_{Ga} defects are N_{D1}, N_{D2}, N_{D3}, N_{A1} and N_{A2}, respectively. For n-type GaN with the Fermi level pinned at the D1 (0/+) level, inequality $N_{D1} > N_{A1} + N_{A2}$ holds. As the concentrations of acceptors increase, the Fermi level shifts to the A2 levels and stays there while inequality $N_{A2} > N_{A1} - N_{D1}$ is valid. In both cases the YL_{Be} band is strong because photogenerated holes are quickly captured by the excited state (at 0.3 eV above the VBM) of the negatively charged Be_{Ga}-

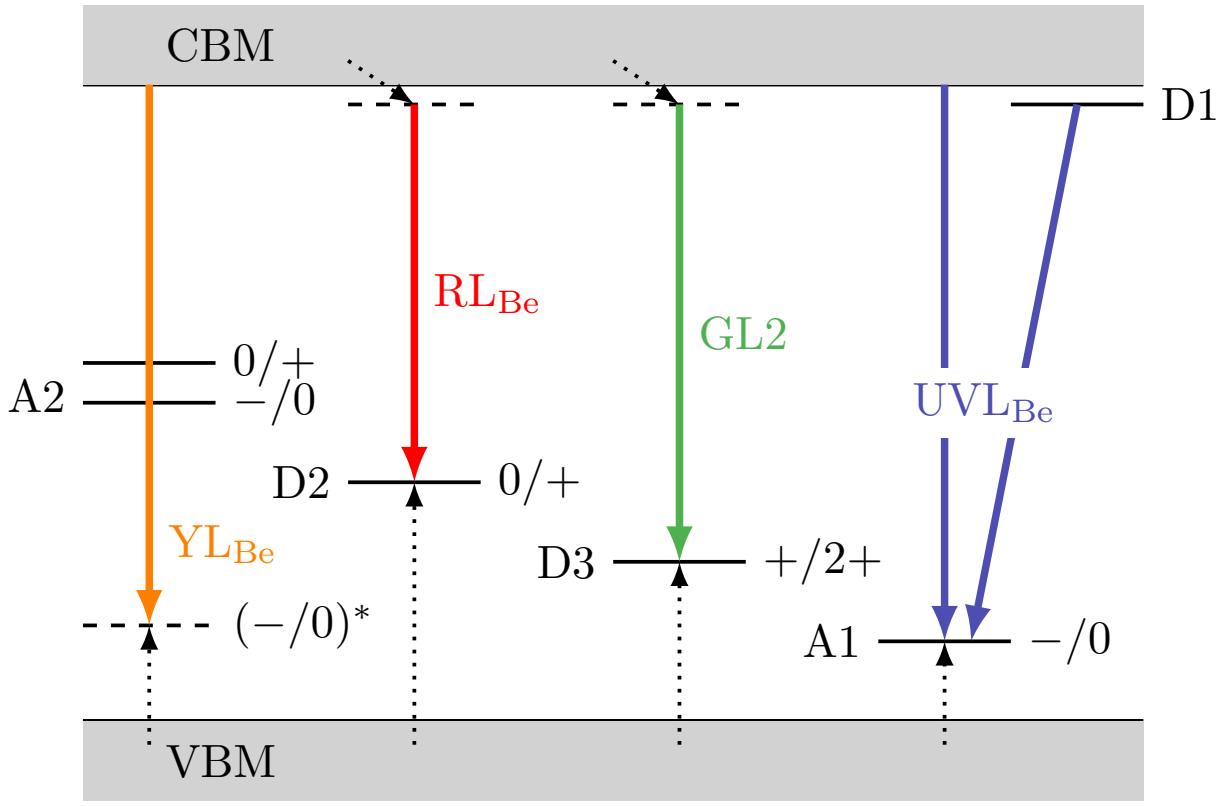

FIG. 17. (Color online) Band diagram with transition levels for the shallow O_N donor (D1), Be_{Ga}-V_N complex (D2), V_N (D3), Be_{Ga} acceptor (A1), and Be_{Ga}-V_N-Be_{Ga} complex (A2). Radiative and nonradiative transitions are shown with wavy and dotted lines, respectively.

V_N-Be_{Ga} acceptors. A strong UVL_{Be} band is observed in samples annealed at 900 °C to activate the acceptors, yet the concentration of the isolated Be_{Ga} acceptors is lower than that of the Be_{Ga}-V_N-Be_{Ga} complexes (Table. I). The RL_{Be} and GL2 bands are weak because donors are less efficient in capturing holes. Further, the Fermi level is pinned at the D2 level in samples with $N_{A2} < N_{A1} - N_{D1}$. The sharp transition of the Fermi level from D2 and A2 occurs when N_{A2} exceeds $(N_{A1} - N_{D1})$. It may happen in the same samples where these concentrations are very close to each other and gradient of the concentrations exist. The conclusions are valid in a more general situation where N_{A1} represents all acceptors with transition levels below A2 and N_{D1} represents all donors with transition levels above A2. As $N_{A2} < N_{A1} - N_{D1}$, all the Be_{Ga}-V_N-Be_{Ga} defects are positively charged, the acceptor excited state disappears, and no YL_{Be} band can be observed. Note that recombination pathways are difficult to predict in semi-insulating semiconductors where nonlinear effects may lead to population inversion at low temperatures and tunable thermal quenching [35].

Accoridng to the model proposed in Ref. [35], the most efficient recombination channelas are characterized by the fastest capture of holes below the critical temperature T_0, while recombination channels with the fastest capture of electrons dominate above T_0. The abrupt and tunable quenching of the YL_{Be} band (Sec. III D) indicates that this band, as a very efficient hole trap, is strong in samples where the hole capture determines PL intensities. On the other hand, the RL_{Be} and GL2 bands are strong in samples where the electron capture determines PL intensities. The related donors quickly capture photogenerated electrons thanks to the excited states close to the conduction band. Thus, a sharp boundary between the "yellow" and "red" regions in samples 0406b and 0410b (examples of PL spectra are shown in Fig. 2) can be explained by gradual change of the defect concentrations, which may result in an abrupt shift of the Fermi level, similar to what was observed in Ref. [21].

IV. CONCLUSIONS

The experimental PL spectra from GaN:Be samples grown by MBE contain four major PL bands: ultraviolet UVL_{Be}, yellow YL_{Be}, red RL_{Be}, and green GL2. The UVL_{Be} band is caused by the electronic transitions from the conduction band (or shallow donors) to the $0/-$ shallow level of the Be_{Ga} acceptor located at 113 meV above the valence band. The quenching of the UVL_{Be} band (which was observed only in semi-insulating samples) is tunable by the excitation intensity.

The GL2 band is caused by the V_N defects, and it appears only when the YL_{Be} is absent and usually together with the stronger RL_{Be} band. The YL_{Be} is attributed to the Be_{Ga}-V_N-Be_{Ga} acceptor. Its $0/-$ level is calculated at 1.5 eV above the VBM. To explain the experimental results, we propose that the negatively charged Be_{Ga}-V_N-Be_{Ga} acceptor forms an excited state for the hole at 0.3 eV above the VBM. The radiative transitions of electrons from the conduction band to this level are more efficient than nonradiative transitions via the ground state, and the former cause the YL_{Be} band. In n-type GaN:Be, the YL_{Be} band is quenched by the Schön-Klasens mechanism and reveals the ionization energy of 0.3 eV and the hole-capture coefficient of 4×10^{-7} cm^3/s. In semi-insulating GaN:Be samples, the YL_{Be} band is quenched by the abrupt and tunable quenching mechanism, and the quenching behavior agrees with above-mentioned parameters.

The RL_{Be} band is attributed to the Be_{Ga}-V_N donor with the $+/0$ level located at 0.95 eV

above the VBM. First, a photogenerated hole is captured at this level, and the hydrogenic Coulomb excited state is formed near the conduction band. A free electron is captured by this state. Finally, the electron and hole recombine (the internal transition) to produce the RL_{Be} band. The decay of the RL_{Be} intensity after a laser pulse is exponential, and the characteristic PL lifetime (about 2 μs) is weakly dependent on temperature between 18 and 200 K.

ACKNOWLEDGMENTS

This work was supported by the National Science Foundation (DMR-1904861), and by the VCU PeRQ Fund. All calculations were performed at the VCU Center for High Performance Computing. The authors are grateful to T. H. Myers of Texas State University for providing the samples.

---

[1] H. Morkoç, *Handbook of Nitride Semiconductors and Devices, Electronic and Optical Processes in Nitrides* (John Wiley & Sons, 2009).

[2] M. A. Reshchikov, P. Ghimire, and D. O. Demchenko, Phys. Rev. B **97**, 205204 (2018).

[3] K. H. Ploog and O. Brandt, J. of Vac. Sci. Tech. A: Vacuum, Surfaces, and Films **16**, 1609 (1998).

[4] S. Sugita, Y. Watari, G. Yoshizawa, J. Sodesawa, H. Yamamizu, K.-T. Liu, Y.-K. Su, and Y. Horikoshi, Jpn. J. Appl. Phys. **42**, 71 (2003).

[5] T. M. Al Tahtamouni, A. Sedhain, J. Y. Lin, and H. X. Jiang, Jordan Journal of Physics **3**, 77 (2010).

[6] C.-C. Yu, C. F. Chu, J. Y. Tsai, C. F. Lin, and S. C. Wang, J. Appl. Phys. **92**, 1881 (2002).

[7] D. Demchenko, M. Vorobiov, O. Andrieiev, T. Myers, and M. Reshchikov, Phys. Rev. Lett. **126**, 027401 (2021).

[8] F. Tuomisto, V. Prozheeva, I. Makkonen, T. H. Myers, M. Bockowski, and H. Teisseyre, Phys. Rev. Lett. **119**, 196404 (2017).

[9] F. Mireles and S. E. Ulloa, Phys. Rev. B **58**, 3879 (1998).

[10] H. Wang and A.-B. Chen, Phys. Rev. B **63**, 125212 (2001).

[11] C. G. Van de Walle, S. Limpijumnong, and J. Neugebauer, Phys. Rev. B **63**, 245205 (2001).

[12] C. D. Latham, R. M. Nieminen, C. J. Fall, R. Jones, S. Öberg, and P. R. Briddon, Phys. Rev. B **67**, 205 (2003).

[13] X. Cai, J. Yang, P. Zhang, and S.-H. Wei, Phys. Rev. Applied **11**, 034019 (2019).

[14] J. L. Lyons, A. Janotti, and C. G. Van de Walle, Jpn. J. Appl. Phys. **52**, 08JJ04 (2013).

[15] S. Pekar, Usp. Fiz. Nauk **50**, 197 (1953).

[16] J. L. Lyons, A. Janotti, and C. G. Van de Walle, J. Appl. Phys. **115**, 012014 (2014).

[17] B. J. Skromme, G. L. Martinez, L. Krasnobaev, and D. B. Poker, MRS Online Proceedings Library **639**, 1139 (2001).

[18] H. Teisseyre, J. L. Lyons, A. Kaminska, D. Jankowski, D. Jarosz, M. Boćkowski, A. Suchocki, and C. G. Van de Walle, J. Phys. D: Appl. Phys. **50**, 22LT03 (2017).

[19] M. Lamprecht, K. Thonke, H. Teisseyre, and M. Boćkowski, Phys. Stat. Sol. (b) **255**, 1800126 (2018).

[20] K. Lee, B. L. Van Mil, M. Luo, L. Wang, N. C. Giles, and T. H. Myers, Phys. Stat. Sol (c) **2**, 2204 (2005).

[21] M. A. Reshchikov, D. O. Demchenko, J. D. McNamara, S. Fernández-Garrido, and R. Calarco, Phys. Rev. B **90**, 035207 (2014).

[22] A. J. Ptak, T. H. Myers, L. Wang, N. C. Giles, M. Moldovan, C. R. D. Cunha, L. A. Hornak, C. Tian, R. A. Hockett, S. Mitha, and P. Van Lierde, MRS Online Proceedings Library Archive **639**, 10.1557/PROC-639-G3.3 (2000).

[23] K. Lee, *Issues for p-type doping of gallium nitride with beryllium and magnesium grown by rf-plasma assisted molecular beam epitaxy*, Ph.D., West Virginia University, United States – West Virginia (2007).

[24] M. A. Reshchikov, M. Vorobiov, D. O. Demchenko, U. Özgür, H. Morkoç, A. Lesnik, M. P. Hoffmann, F. Hörich, A. Dadgar, and A. Strittmatter, Phys. Rev. B **98**, 125207 (2018).

[25] M. A. Reshchikov, J. Appl. Phys. **129**, 121101 (2021).

[26] J. Heyd, G. E. Scuseria, and M. Ernzerhof, J. Chem. Phys. **118**, 8207 (2003).

[27] D. O. Demchenko, I. C. Diallo, and M. A. Reshchikov, Phys. Rev. B **97**, 205 (2018).

[28] C. Freysoldt, J. Neugebauer, and C. G. Van de Walle, Phys. Rev. Lett. **102**, 016402 (2009).

[29] C. Freysoldt, J. Neugebauer, and C. G. Van de Walle, Phys. Stat. Sol. (b) **248**, 1067 (2011).

[30] C. Freysoldt, B. Grabowski, T. Hickel, J. Neugebauer, G. Kresse, A. Janotti, and C. G. Van de

Walle, Rev. Mod. Phys. **86**, 253 (2014).

[31] D. O. Demchenko and M. A. Reshchikov, Appl. Phys. Lett. **118**, 142103 (2021).

[32] P. Yu and M. Cardona, *Fundamentals of semiconductors: physics and materials properties* (Springer Science & Business Media, 2010).

[33] M. A. Reshchikov and H. Morkoç, J. Appl. Phys. , 96 (2005).

[34] K. Kornitzer, T. Ebner, K. Thonke, R. Sauer, C. Kirchner, V. Schwegler, M. Kamp, M. Leszczynski, I. Grzegory, and S. Porowski, Phys. Rev. B **60**, 1471 (1999).

[35] M. A. Reshchikov, A. A. Kvasov, M. F. Bishop, T. McMullen, A. Usikov, V. Soukhoveev, and V. A. Dmitriev, Phys. Rev. B **84**, 075212 (2011).

[36] M. A. Reshchikov, Phys. Stat. Sol. (a) **218**, 2000101 (2021).

[37] J. F. Muth, J. H. Lee, I. K. Shmagin, R. M. Kolbas, H. C. Casey, B. P. Keller, U. K. Mishra, and S. P. DenBaars, Appl. Phys. Lett. **71**, 25722574 (1997).

[38] M. A. Reshchikov, Phys. Rev. B **85**, 245203 (2012).

[39] R. Y. Korotkov, M. A. Reshchikov, and B. W. Wessels, Physica B: Condensed Matter **325**, 1 (2003).

[40] M. A. Reshchikov, J. D. McNamara, M. Toporkov, V. Avrutin, H. Morkoç, A. Usikov, H. Helava, and Y. Makarov, Scientific Reports **6**, 37511 (2016).

[41] M. A. Reshchikov, A. Usikov, H. Helava, Y. Makarov, V. Prozheeva, I. Makkonen, F. Tuomisto, J. H. Leach, and K. Udwary, Scientific Reports **7**, 9297 (2017).

[42] H. Teisseyre, M. Boćkowski, I. Grzegory, A. Kozanecki, B. Damilano, Y. Zhydachevskii, M. Kunzer, K. Holc, and U. T. Schwarz, Appl. Phys. Lett. **103**, 011107 (2013).

[43] M. D. McCluskey and E. E. Haller, *Dopants and defects in semiconductors* (CRC press, 2018).

[44] D. M. Hofmann, B. K. Meyer, H. Alves, F. Leiter, W. Burkhard, N. Romanov, Y. Kim, J. Krüger, and E. R. Weber, Phys. Stat. Sol. (a) **180**, 261 (2000).

[45] M. A. Reshchikov and H. Morkoç, MRS Online Proceedings Library Archive **831**, 10.1557/PROC-831-E3.7 (2004).

[46] M. A. Reshchikov, R. M. Sayeed, U. Özgür, D. O. Demchenko, J. D. McNamara, V. Prozheeva, F. Tuomisto, H. Helava, A. Usikov, and Y. Makarov, Phys. Rev. B **100**, 045204 (2019).